Shock compression of helium to 360 GPa

M. Wadas,[1,*] S. Brygoo,[2] P. Loubeyre,[2] P. M. Celliers,[3] G. W. Collins,[4] J. H. Eggert,[3] R. Jeanloz,[5] E. Johnsen,[1] B. Militzer,[5] J. R. Rygg,[4] and M. Millot[3]

[1] *University of Michigan, Ann Arbor, Michigan 48109*
[2] *Commissariat à l'Énergie Atomique, DAM/DIF, Bruyéres-le-Châtel, France*
[3] *Lawrence Livermore National Laboratory, Livermore, CA 94550, USA*
[4] *Departments of Mechanical Engineering, Physics and Astronomy, and the Laboratory of Laser Energetics, University of Rochester, Rochester, NY 14623, USA*
[5] *Departments of Earth and Planetary Science and Astronomy, University of California, Berkeley, CA 94720, USA*

Hugoniot data are obtained for helium from 270-360 GPa, nearly doubling the pressure of previous experimental measurements. The helium samples are first precompressed to 2.8-3.4 times ambient-pressure cryogenic liquid density in a diamond anvil cell prior to laser-driven shock compression at the Omega Laser Facility. These data show significant reflectivity and greater compressibility compared to the predictions of a range of existing equations of state, which may be caused by the onset of continuous ionization. The data serve as important benchmarks for *ab initio* predictions used to model Jovian interiors and white dwarf atmospheres.

Helium is the second most abundant chemical element in the universe, and characterizing its behavior in high-pressure environments is essential for our understanding of Jovian interiors and white dwarfs [1–6]. In particular, the metallization of helium and its miscibility with hydrogen at megabar-level pressures may have dramatic consequences on the dynamics of the convective barrier thought to exist in the interior of Jupiter separating helium-depleted and helium-rich layers [3, 7–10]. Competing models predict considerably different band-gap closures occurring at $\sim 2\,\mathrm{g\,cm^{-3}}$ [11] and $\sim 10\,\mathrm{g\,cm^{-3}}$ [12], with the latter suggesting that only insulating helium exists within Jupiter, motivating the need for additional experimental data. Moreover, understanding the behavior of high-pressure helium is essential for modeling heat transfer in the helium-rich atmospheres of white dwarfs [13], which enables constraints on models of interior structure and thermal evolution that are highly sensitive to ionization (metallization) behavior [14–17].

In addition to these physics applications, the simplicity of helium makes it an important benchmark for *ab initio* simulations such as density functional theory (DFT), molecular dynamics (MD), and path integral Monte-Carlo (PIMC) calculations, especially at the megabar-level pressures of the notoriously challenging warm dense matter regime [18]. In particular, its monoatomic nature makes helium, as opposed to hydrogen, the simplest element for which pressure- or temperature-induced ionization physics can be isolated from the effects of molecular dissociation [19–29]. While past studies have shown evidence for ionization, the parameter space over which helium ionizes is largely unexplored experimentally [30–32]. Further obfuscating our understanding are discrepancies in the pressure response predicted from existing models [33–37] beyond approximately 100 GPa for shocked helium initially precompressed near 1 GPa, a regime where data are limited to only seven past experiments [11, 38]. Even after reanalysis of these experiments with improved quartz standard models [39], discrepancies with existing models [33–35], including the First-Principles Equation of State (FPEOS) [36], remain, motivating the need for experimental data to elucidate the behavior of helium and discriminate between existing models.

Experimental studies utilized diamond anvil cell (DAC) devices to statically compress helium up to 58 GPa and examined the pressure dependence of the refractive index and melting line [40–43], while experiments using gas-gun facilities to dynamically compress helium with shock waves documented the pressure-density shock equation of state up to 56 GPa [44]. The maximum projectile velocity in such experiments [45], however, limits the pressures that can be achieved. In addition, achievable thermodynamic states are constrained to the material shock Hugoniot, limiting the density that can be achieved. Moreover, the final states are anchored to ambient conditions and therefore lack independent control of pressure and temperature. These challenges are ameliorated through the combination of static and dynamic techniques, where a DAC is used for tailored precompression followed by laser-driven shock compression [46], enabling access to conditions relevant to planetary interiors and white dwarf atmospheres [11, 38, 39].

This work presents data from four experiments at the Omega Laser Facility compressing helium in a DAC from initial static pressures of 0.76-1.20 GPa ($\sim$ 3 times its cryogenic liquid density at ambient pressures) to 270-360 GPa, thereby extending the range of experimental data to a novel regime where predictions from existing equation of state (EOS) models diverge [33–37]. The record pressures were achieved by designing the DAC such that the desired precompressed state could be reached with the thinnest front diamond window possible (200 µm), efficiently coupling the pressure from the 1 ns-optimized laser drive to the sample [47]. The data show increases in reflectivity consistent with continuous

* mwadas@umich.edu

ionization, which is also reflected in the increased compression. The pressure and temperature response is reasonably captured by FPEOS, resolving past discrepancies [11, 38, 39] and enabling critical insight for the behavior of warm dense helium in Jovian interiors and white dwarf atmospheres.

In each experiment, supercritical fluid helium is compressed in a DAC with a back sapphire window at room temperature using a gas loading system and a ruby for pressure characterization [39, 46, 48]. In order of increasing precompression, the experiments are referred to as S74727, S70906, S74722, and S72497 throughout this work with initial densities $\rho_0 = 0.351$, 0.385, 0.390, and $0.422\,\mathrm{g\,cm^{-3}}$, respectively. The DAC setup is similar to those employed by Refs. [10, 46, 49] and is shown schematically in Fig. 1(a). A quartz impedance standard [50, 51] sits at the base of the diamond, and a thin layer of gold shields the DAC from radiation from the laser-driven side of the target, preventing preheat and photoionization. Additional details about target preparation and the characterization of the initial state are provided in the supplemental material [52]. Ten or twelve lasers are used to generate a 1 ns square pulse delivering between 3.9 and 5.5 kJ of ultraviolet radiation at 351 nm to the plastic ablator, driving a shock wave into the DAC which subsequently passes through the quartz standard and into the helium sample, as shown schematically in Fig. 1(b).

The reflective, self-emitting shock front is tracked using the line-imaging velocity interferometer for any reflector (VISAR) system at the Omega Laser Facility [53, 54], generating the raw data shown in Fig. 1(c). Shifts in the VISAR fringes are proportional to changes in the apparent shock velocity, U_{ap}, which is related to the actual shock velocity, $U_s = U_{ap}/n$, where n is the material index of refraction. The effect of precompression on the indices of refraction of quartz [55] and helium [56] is considered for an accurate velocity measurement. Despite the use of anti-reflective coatings, the VISAR signal is influenced by reflections from stationary interfaces, the treatment of which is detailed in the supplemental material [52]. As the shock wave passes from the quartz to the helium, it sets the interface into motion at velocity U_p, and the difference in shock impedance causes the transmitted shock wave to have a different velocity, resulting in a discontinuous shift in the VISAR fringes. The ambiguity in determining the absolute fringe shift is resolved through the use of two VISAR channels with different fringe sensitivities controlled by different etalon thicknesses ($16.0829\,\mathrm{km\,s^{-1}}$ per fringe for the 3.096 mm etalon and $6.9065\,\mathrm{km\,s^{-1}}$ per fringe for the 7.2095 mm etalon). Any remaining ambiguity is resolved by matching the time-integrated shock velocity through the quartz layer to its known thickness.

Because the particle velocity and pressure on either side of the shocked interface between the quartz and helium are equal, the known response of the quartz standard to the high-pressure loading can be used to determine the state in the shocked helium using standard

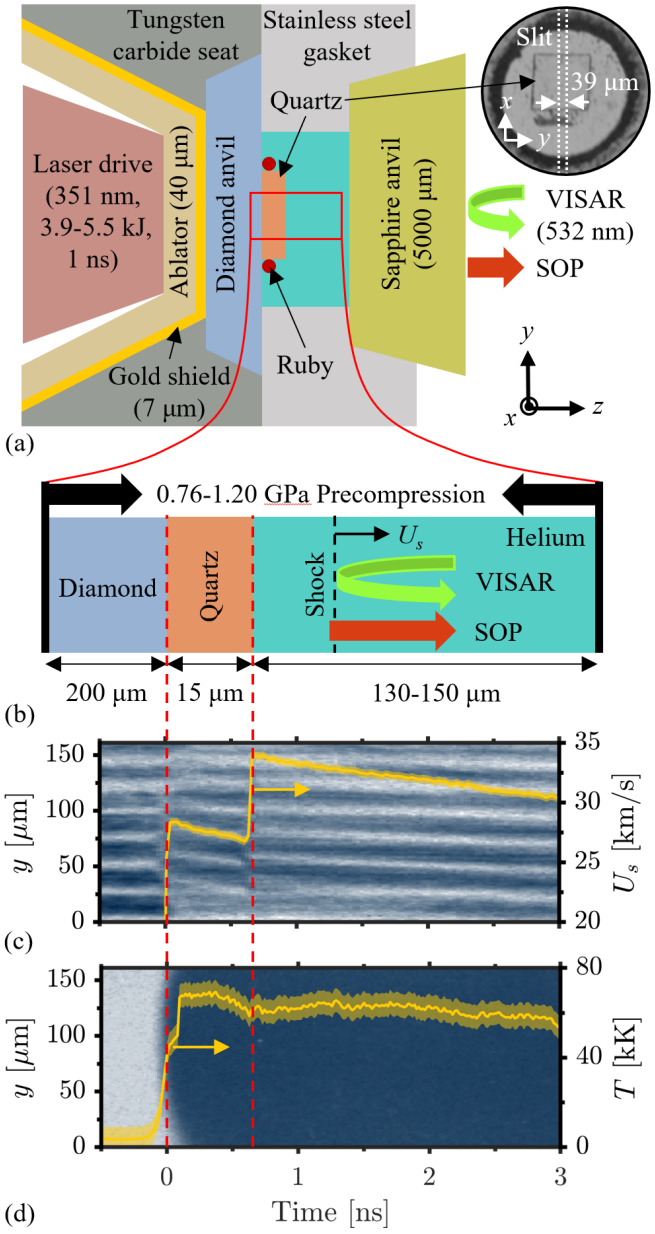

FIG. 1. (a) A schematic showing the geometry of the diamond anvil cell (DAC) used in the present work, including a micrograph (right) of the pressure chamber showing the quartz reference plate and the projection of the VISAR streak camera entrance slit onto the target (white-dashed lines) for S74722. (b) A close-up of the schematic in (a) detailing the sample geometry, precompression, and shock transit. (c) The velocity interferometer for any reflector (VISAR) data vs. time with overlaid shock velocity (yellow line) from S74722. The transition of the shock between materials is clearly seen as a discontinuous jump in the shock velocity. (d) The streaked optical pyrometry (SOP) data vs. time with overlaid temperature (yellow line) from S74722. In (c,d), the shaded yellow region indicates measurement error (see supplemental material [52]).

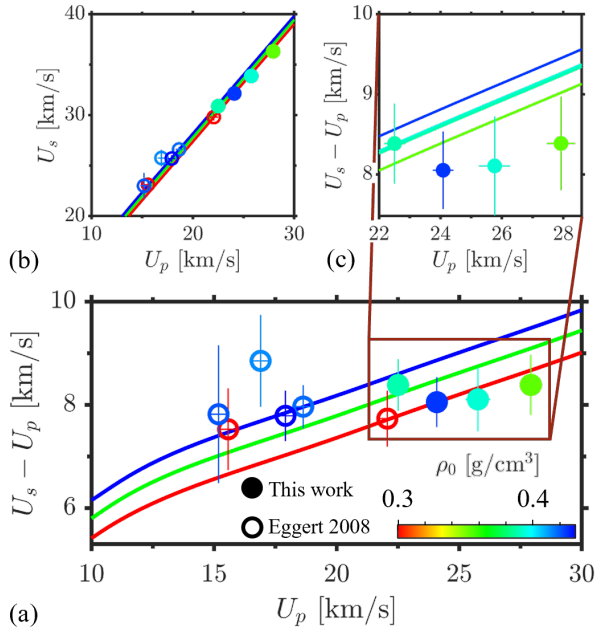

FIG. 2. (a) The difference between the shock and particle velocity vs. particle velocity in helium for the present work (closed symbols) and past work (open symbols) [11, 38, 39]. Color indicates the precompressed density. Three FPEOS Hugoniot curves [19, 22, 36] spanning the range of initial densities in the experimental data ($\rho_0 = 0.296\,\mathrm{g\,cm^{-3}}$, $0.362\,\mathrm{g\,cm^{-3}}$, and $0.429\,\mathrm{g\,cm^{-3}}$) are shown. (b) The shock velocity vs. particle velocity. (c) Close-up view of the new data with an expanded color scale and Hugoniot curves matching the precompression of each corresponding experiment.

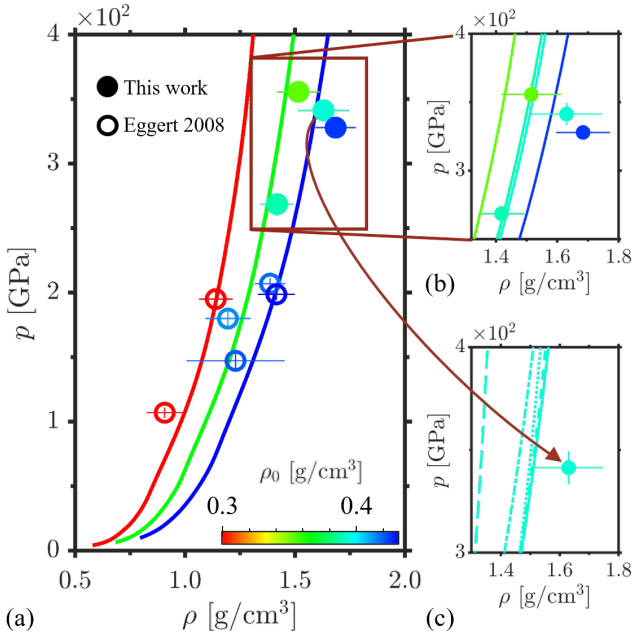

FIG. 3. (a) The pressure vs. density in helium for the present work (closed symbols) and past work (open symbols) [11, 38, 39]. Color indicates the precompressed density. Three FPEOS Hugoniot curves [36] spanning the range of initial densities in the experimental data ($\rho_0 = 0.296\,\mathrm{g\,cm^{-3}}$, $0.362\,\mathrm{g\,cm^{-3}}$, and $0.429\,\mathrm{g\,cm^{-3}}$) are shown. (b) Close-up view of the new data with an expanded color scale and Hugoniot curves matching the precompression of each corresponding experiment. (c) S74722 with Hugoniot curves, in order of increasing density, from LEOS20 (long-dashed) [33], SESAME3764 (dash-dotted), SESAME3761 (dotted) [34], REOS (short-dashed) [35], and FPEOS (solid) [19, 22, 36].

impedance matching techniques, detailed in the supplemental material [52]. The key measurement enabling the state calculation is the velocity of the shock in quartz and helium immediately before and after, respectively, the shock breaks out into the helium. The agreement between the two VISAR measurements before and following the breakout is used to determine the measurement error, as described in the supplemental material [52]. Figure 2 shows the shock velocity in helium vs. the particle velocity for the new data and existing data from Refs. [11, 38, 39] exploring shocked helium precompressed between 0.51 and 1.25 GPa. We restrict our attention to this narrow range of precompressed densities to enable a detailed comparison between the data and predictions from existing models. A larger data set is provided in the supplemental material [52]. In general, the new data show good agreement with predictions from FPEOS, an EOS database that combines results from PIMC and DFT-MD simulations [36].

With the calculated velocities in quartz and helium known, the Rankine-Hugoniot relations are used to determine the pressure and density downstream of the shock in the helium [39, 57], as shown in Fig. 3, again alongside past data and predictions from FPEOS. The data indicate pressures near and in excess of 350 GPa and again show good agreement with FPEOS, as seen in the upper-right panel. The three highest-pressure experiments show greater compression than the prediction of FPEOS, but still fall within, or very nearly within, the experimental error bars. Fig. 3(c) also shows the predicted Hugoniot curves for S74722 from the tabular equation of state models LEOS20 [33], SESAME3761 [34], and SESAME3764 [58]. These models combine a variety of physical assumptions to define the free energy over wide ranges of density and temperature that are adjusted to match selected experimental observations. The data are also compared to predictions from REOS, a broad-range free-energy model fit to DFT-MD simulations [35]. The prediction of these EOS models for S74727, S70906, and S72497 show similar trends. Of these models, FPEOS is the most compressible and therefore results in better agreement with the experiments. The greater compressibility may be related to an increase in the internal molecular degrees of freedom due to the onset of ionization [19, 21, 22, 36], which is further elucidated by reflectivity measurements discussed next.

While the phase of the VISAR signal enables a velocity measurement, the amplitude encodes information

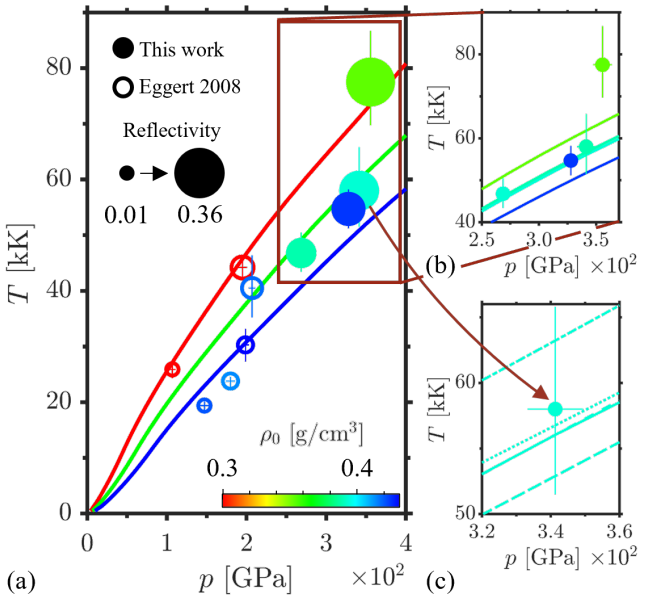

FIG. 4. (a) The temperature vs. pressure in helium for the present work (closed symbols) and past work (open symbols) [11, 38, 39]. Color indicates the precompressed density, while the symbol size indicates reflectivity. Three FPEOS Hugoniot curves [36] spanning the range of initial densities in the experimental data (ρ_0 = 0.296 g/cm^3, 0.362 g/cm^3, and 0.429 g/cm^3) are shown. (b) Close-up view of the new data with an expanded color scale and Hugoniot curves matching the precompression of each corresponding experiment. (c) S74722 with Hugoniot curves from LEOS20 (long-dashed) [33], SESAME3764 (dash-dotted), SESAME3761 (dotted) [34], REOS (short-dashed) [35], and FPEOS (solid) [19, 22, 36].

that can be used to determine the shock reflectivity in helium at the laser wavelength of 532 nm, where the signal in quartz again acts as a measurement standard [59]. Accounting for changes in the index of refraction resulting from precompression [39, 60], we calculate shock front reflectivity in helium in excess of 35% (data for each experiment and a description of the error analysis is provided in the supplemental material [52]), as indicated by the size of the data points in Fig. 4. The measured reflectivity is almost twice that of past experiments [11, 38], consistent with the enhanced compressibility observed in Fig. 3 and the onset of ionization.

Figure 4 also shows the temperature downstream of the shock in helium inferred from streaked optical pyrometry (SOP) data, an example of which is shown in Fig. 1(d), where the slight increase in the signal intensity immediately following the breakout of the shock into the helium is likely caused by space-time distortions and nonlinearity in the diagnostic sweep rate [61, 62]. Combined with the measured reflectivity, the spectral radiance measured with SOP can be used to infer the shock temperature using the grey-body radiation approximation [61], with details provided in the supplemental material [52]. In the present experiments, the shock speed in quartz exceeds the range over which we have qualified quartz as a temperature standard in precompressed targets [39], reaching a higher temperature regime where the apparent shock temperature rises linearly with increasing shock speed [60, 63] instead of the power scaling observed at shock velocities from 10 km s^{-1} to 20 km s^{-1} [39, 59]. Extending the precompressed reference model to this regime is beyond the scope of the present work, but given that the initial precompression is limited to approximately $\sim$ 1 GPa, we use the ambient density curve valid beyond 20 km s^{-1} and add a correction for the precompression effect, detailed in the supplemental material [52].

The agreement between the prediction of FPEOS and the data is generally good, as seen in the upper right panel of Fig. 4. The temperature measurement for S74727 is found to be higher than the prediction of FPEOS, but the grey-body temperature value may be artificially high due to a possible overprediction of the reflectivity from our experimental fit to the present and preexisting data [11, 38, 39] (see supplemental material [52]). As in Fig. 3, the lower-right panel also shows predictions from LEOS20, SESAME3764, SESAME3761, and REOS for S74722. The temperature measurements further enable a prediction of conductivity according to the Drude-like model of Ref. [12], giving 263, 93, 145, and 126 kS m^{-1} for S74727, S70906, S74722, and S72497, respectively (see supplemental material [52]), exceeding previous measurements by up to a factor of 2 and providing further evidence of the increasing ionization in the present pressure regime.

Four experiments achieved a novel state in warm, dense fluid helium and show evidence of continuous ionization [17, 21, 22, 30], with measured reflectivity in excess of 35% over pressures ranging from 270 to 360 GPa. The increased compression likely caused by the onset of ionization [19] is captured by FPEOS, affirming the ability of first-principles techniques like PIMC and DFT-MD to predict the EOS of warm dense helium in a regime where ionization becomes important. Additional experiments utilizing greater precompression are ongoing to further document the effect of density and temperature on the insulator-to-metal transition in warm dense fluid helium.

ACKNOWLEDGMENTS

This work is supported by the Lawrence Livermore National Laboratory under Subcontract No. B632749 and the U. S. Department of Energy (DOE) as part of the Stewardship Science Graduate Fellowship Program under Grant No. De-NA0003960. Part of this work was performed under the auspices of the US DOE by Lawrence Livermore National Laboratory (LLNL) under contract DE-AC52-07NA27344 and supported by LLNL LDRD Program No. 19-ERD-031. VISAR and SOP

data in this work were analyzed with LLNL Analyze-VISAR code. In addition, funding for this research was provided by the Center for Matter at Atomic Pressures (CMAP), a National Science Foundation (NSF) Physics Frontiers Center, under Award PHY2020249. This material is partially supported by the Department of Energy, Office of Science, Fusion Energy Sciences under Award No. DESC0020340.

[1] P. J. Kortbeek and J. A. Schouten. Equation of state of fluid helium to very high pressure. *Chem. Phys.*, 95(6):4519–4524, 1991.

[2] J. M. McMahon, M. A. Morales, C. Pierleoni, and D. M. Ceperley. The properties of hydrogen and helium under extreme conditions. *Rev. Mod. Phys.*, 84(4):1607, 2012.

[3] B. Militzer, F. Soubiran, S. M. Wahl, and W. Hubbard. Understanding Jupiter's interior. *J. Geophys. Res. Planets*, 121(9):1552–1572, 2016.

[4] G Chabrier, S Mazevet, and François Soubiran. A new equation of state for dense hydrogen–helium mixtures. *The Astrophysical Journal*, 872(1):51, 2019.

[5] D. Saumon, S. Blouin, and P.-E. Tremblay. Current challenges in the physics of white dwarf stars. *Phys. Rep.*, 988:1–63, 2022.

[6] Burkhard Militzer, William B Hubbard, Sean Wahl, Jonathan I Lunine, Eli Galanti, Yohai Kaspi, Yamila Miguel, Tristan Guillot, Kimberly M Moore, Marzia Parisi, et al. Juno spacecraft measurements of jupiter's gravity imply a dilute core. *The planetary science journal*, 3(8):185, 2022.

[7] L. Stixrude and R. Jeanloz. Fluid helium at conditions of giant planetary interiors. *Proc. Natl. Acad. Sci.*, 105(32):11071–11075, 2008.

[8] F. Soubiran, S. Mazevet, C. Winisdoerffer, and G. Chabrier. Optical signature of hydrogen-helium demixing at extreme density-temperature conditions. *Phys. Rev. B*, 87(16):165114, 2013.

[9] J. Zheng, Q. .F Chen, Y. J. Gu, J. T. Li, Z. G. Li, C. J. Li, and Z. Y. Chen. Shock-adiabatic to quasi-isentropic compression of warm dense helium up to 150 GPa. *Phys. Rev. B*, 95(22):224104, 2017.

[10] S. Brygoo, P. Loubeyre, M. Millot, J. R. Rygg, P. M. Celliers, J. H. Eggert, R. Jeanloz, and G. W. Collins. Evidence of hydrogen- helium immiscibility at Jupiter-interior conditions. *Nature*, 593(7860):517–521, 2021.

[11] P. M. Celliers, P. Loubeyre, J. H. Eggert, S. Brygoo, R. S. McWilliams, D. G. Hicks, T. R. Boehly, R. Jeanloz, and G. W. Collins. Insulator-to-conducting transition in dense fluid helium. *Phys. Rev. Lett.*, 104(18):184503, 2010.

[12] F. Soubiran, S. Mazevet, C. Winisdoerffer, and G. Chabrier. Helium gap in the warm dense matter regime and experimental reflectivity measurements. *Phys. Rev. B*, 86(11):115102, 2012.

[13] S. A. Khairallah and B. Militzer. First-principles studies of the metallization and the equation of state of solid helium. *Phys. Rev. Lett.*, 101(10):106407, 2008.

[14] P. Bergeron, D. Saumon, and F. Wesemael. New model atmospheres for very cool white dwarfs with mixed H/He and pure He compositions. *Astrophys. J.*, 443:764–779, 1995.

[15] C. A. Iglesias, F. J. Rogers, and D. Saumon. Density effects on the opacity of cool helium white dwarf atmospheres. *Astrophys. J.*, 569(2):L111, 2002.

[16] P. M. Kowalski, S. Mazevet, D. Saumon, and M. Challacombe. Equation of state and optical properties of warm dense helium. *Phys. Rev. B*, 76(7):075112, 2007.

[17] M. Preising and R. Redmer. Metallization of dense fluid helium from ab initio simulations. *Phys. Rev. B*, 102(22):224107, 2020.

[18] Tobias Dornheim, Zhandos A Moldabekov, Kushal Ramakrishna, Panagiotis Tolias, Andrew D Baczewski, Dominik Kraus, Thomas R Preston, David A Chapman, Maximilian P Böhme, Tilo Döppner, et al. Electronic density response of warm dense matter. *Physics of Plasmas*, 30(3):032705, 2023.

[19] B Militzer. First principles calculations of shock compressed fluid helium. *Phys. Rev. Lett.*, 97(17):175501, 2006.

[20] A. Kietzmann, B. Holst, R. Redmer, M. P. Desjarlais, and T. R. Mattsson. Quantum molecular dynamics simulations for the nonmetal-to-metal transition in fluid helium. *Phys. Rev. Lett.*, 98(19):190602, 2007.

[21] B. Militzer. Path integral Monte Carlo and density functional molecular dynamics simulations of hot, dense helium. *Phys. Rev. B*, 79(15):155105, 2009.

[22] B. Militzer. Correlations in hot dense helium. *J. Phys. A: Math. Theor.*, 42(21):214001, 2009.

[23] C. Winisdoerffer and G. Chabrier. Free-energy model for fluid helium at high density. *Phys. Rev. E*, 71(2):026402, 2005.

[24] A. Becker, W. Lorenzen, J. J. Fortney, N. Nettelmann, M. Schöttler, and R. Redmer. Ab initio equations of state for hydrogen (H-REOS. 3) and helium (He-REOS. 3) and their implications for the interior of brown dwarfs. *Astrophys. J. Suppl. Ser.*, 215(2):21, 2014.

[25] M. Preising, W. Lorenzen, A. Becker, R. Redmer, M. D. Knudson, and M. P. Desjarlais. Equation of state and optical properties of warm dense helium. *Phys. Plasmas*, 25(1):012706, 2018.

[26] Z.-G. Li, Y. Cheng, Q.-F. Chen, and X.-R. Chen. Equation of state and transport properties of warm dense helium via quantum molecular dynamics simulations. *Phys. Plasmas*, 23(5):052701, 2016.

[27] M. Ross and D. A. Young. Helium at high density. *Phys. Lett. A*, 118(9):463–466, 1986.

[28] M. A. Mochalov, R. I. Il'kaev, V. E. Fortov, A. L. Mikhailov, V. A. Arinin, A. O. Blikov, S. E. Elfimov, V. A. Komrakov, V. A. Ogorodnikov, and A. V. Ryzhkov. Thermodynamic parameters of helium under shock-wave and quasi-isentropic compressions at pressures up to 4800 GPa and compression ratios up to 900. *J. Exp. Theor. Phys.*, 125(5):948–963, 2017.

[29] V. K. Gryaznov, I. L. Iosilevskiy, and V. E. Fortov. Thermodynamics of hydrogen and helium plasmas in megabar and multi-megabar pressure range under strong shock and isentropic compression. *plasma Phys. Control. Fusion*, 58(1):014012, 2015.

[30] M. Preising and R. Redmer. Nonmetal-to-metal tran-

sition in dense fluid helium. *Contrib. to Plasma Phys.*, 61(10):e202100105, 2021.

[31] A. Förster, T. Kahlbaum, and W. Ebeling. Equation of state and the phase diagram of dense fluid helium in the region of partial ionization. *Laser Part. Beams*, 10(2):253–262, 1992.

[32] V. D. Urlin. Equations of state and the phase diagram of dielectric and metallic helium-4. *J. Exp. Theor. Phys.*, 127(1):121–130, 2018.

[33] R. M. More, K. H. Warren, D. A. Young, and G. B. Zimmerman. A new quotidian equation of state (QEOS) for hot dense matter. *The Physics of fluids*, 31(10):3059–3078, 1988.

[34] S. P. Lyon. Sesame: the Los Alamos National Laboratory equation of state database. *Los Alamos National Laboratory report LA-UR-92-3407*, 1992.

[35] N. Nettelmann, B. Holst, A. Kietzmann, M. French, R. Redmer, and D. Blaschke. Ab initio equation of state data for hydrogen, helium, and water and the internal structure of Jupiter. *Astrophys. J.*, 683(2):1217, 2008.

[36] B. Militzer, F. González-Cataldo, S. Zhang, K. P. Driver, and F. Soubiran. First-principles equation of state database for warm dense matter computation. *Phys. Rev. E*, 103(1):013203, 2021.

[37] D. Saumon. Evaluation of helium equation of state tables. Technical report, Los Alamos National Lab.(LANL), Los Alamos, NM (United States), 2020.

[38] J. Eggert, S. Brygoo, P. Loubeyre, R. S. McWilliams, P. M. Celliers, D. G. Hicks, T. R. Boehly, R. Jeanloz, and G. W. Collins. Hugoniot data for helium in the ionization regime. *Phys. Rev. Lett.*, 100:124503, Mar 2008.

[39] S. Brygoo, M. Millot, P. Loubeyre, A. E. Lazicki, S. Hamel, T. Qi, et al. Analysis of laser shock experiments on precompressed samples using a quartz reference and application to warm dense hydrogen and helium. *J. Appl. Phys.*, 118(19):195901, 2015.

[40] P. Loubeyre, J. M. Besson, J. P. Pinceaux, and J. P. Hansen. High-pressure melting curve of ^{4}He. *Phys. Rev. Lett.*, 49:1172–1175, Oct 1982.

[41] R. Le Toullec, P. Loubeyre, and J.-P. Pinceaux. Refractive-index measurements of dense helium up to 16 GPa at T=298 K: Analysis of its thermodynamic and electronic properties. *Phys. Rev. B*, 40:2368–2378, Aug 1989.

[42] P Loubeyre, R LeToullec, JP Pinceaux, HK Mao, J Hu, and RJ Hemley. Equation of state and phase diagram of solid he 4 from single-crystal x-ray diffraction over a large p-t domain. *Physical review letters*, 71(14):2272, 1993.

[43] W. L. Vos, M. G. E. van Hinsberg, and J. A. Schouten. High-pressure triple point in helium: The melting line of helium up to 240 kbar. *Phys. Rev. B*, 42:6106–6109, Oct 1990.

[44] W. J. Nellis, N. C. Holmes, A. C. Mitchell, R. J. Trainor, G. K. Governo, M. Ross, and D. A. Young. Shock compression of liquid helium to 56 GPa (560 kbar). *Phys. Rev. Lett.*, 53(13):1248, 1984.

[45] AC Mitchell and WJ Nellis. Diagnostic system of the lawrence livermore national laboratory two-stage light-gas gun. *Review of scientific instruments*, 52(3):347–359, 1981.

[46] R. Jeanloz, P. M. Celliers, G. W. Collins, J. H. Eggert, K. M. Lee, R. S. McWilliams, S. Brygoo, and P. Loubeyre. Achieving high-density states through shock-wave loading of precompressed samples. *Proc. Natl. Acad. Sci.*, 104(22):9172–9177, 2007.

[47] M. J. Wadas, G. Cearley, J. Eggert, E. Johnsen, and M. Millot. A theoretical approach for transient shock strengthening in high-energy-density laser compression experiments. *Phys. Plasmas*, 28(8):082708, 2021.

[48] J. C. Chervin, B. Canny, and M. Mancinelli. Ruby-spheres as pressure gauge for optically transparent high pressure cells. *International Journal of High Pressure Research*, 21(6):305–314, 2001.

[49] M. Millot, S. Hamel, J. R. Rygg, P. M. Celliers, G. W. Collins, F. Coppari, D. E. Fratanduono, R. Jeanloz, D. C. Swift, and J. H. Eggert. Experimental evidence for superionic water ice using shock compression. *Nat. Phys.*, 14(3):297–302, 2018.

[50] E. Calderon, M. Gauthier, F. Decremps, G. Hamel, G. Syfosse, and A. Polian. Complete determination of the elastic moduli of α-quartz under hydrostatic pressure up to 1 GPa: an ultrasonic study. *Journal of Physics: Condensed Matter*, 19(43):436228, 2007.

[51] M. P. Desjarlais, M. D. Knudson, and K. R. Cochrane. Extension of the hugoniot and analytical release model of α-quartz to 0.2–3 tpa. *J. Appl. Phys.*, 122(3):035903, 2017.

[52] See supplemental material at [URL will be inserted by publisher] for a description the experimental setup and measurement, analysis, and error details.

[53] P. M. Celliers, D. K. Bradley, G. W. Collins, D. G. Hicks, T. R. Boehly, and W. J. Armstrong. Line-imaging velocimeter for shock diagnostics at the OMEGA laser facility. *Rev. Sci. Instrum.*, 75(11):4916–4929, 2004.

[54] Peter M Celliers and Marius Millot. Imaging velocity interferometer system for any reflector (visar) diagnostics for high energy density sciences. *Review of Scientific Instruments*, 94(1), 2023.

[55] G. Ghosh. Dispersion-equation coefficients for the refractive index and birefringence of calcite and quartz crystals. *Opt. Commun.*, 163(1-3):95–102, 1999.

[56] A. Dewaele, J. H. Eggert, P. Loubeyre, and R. Le Toullec. Measurement of refractive index and equation of state in dense He, H_2, H_2O, and Ne under high pressure in a diamond anvil cell. *Phys. Rev. B*, 67(9):094112, 2003.

[57] M. D. Knudson and M. P. Desjarlais. Shock compression of quartz to 1.6 TPa: Redefining a pressure standard. *Phys. Rev. Lett.*, 103(22):225501, 2009.

[58] G. I. Kerley. An equation of state for helium. Technical report, 2013.

[59] D. G. Hicks, T. R. Boehly, J. H. Eggert, J. E. Miller, P. M. Celliers, and G. W. Collins. Dissociation of liquid silica at high pressures and temperatures. *Phys. Rev. Lett.*, 97(2):025502, 2006.

[60] M. Millot, N. Dubrovinskaia, A. Černok, S. Blaha, L. Dubrovinsky, D. G. Braun, P. M. Celliers, G. W. Collins, J. H. Eggert, and R. Jeanloz. Shock compression of stishovite and melting of silica at planetary interior conditions. *Science*, 347(6220):418–420, 2015.

[61] J. E. Miller, T. R. Boehly, A. Melchior, D. D. Meyerhofer, P. M. Celliers, J. H. Eggert, D. G. Hicks, C. M. Sorce, J. A. Oertel, and P. M. Emmel. Streaked optical pyrometer system for laser-driven shock-wave experiments on OMEGA. *Rev. Sci. Instrum.*, 78(3):034903, 2007.

[62] M. Fiedler. Modeling streak camera sweep speeds.

[63] E. J. Davies, P. M. Celliers, T. R. Boehly, R. Boni, G. W. Collins, A. Ernesti, et al. Pushing the α-quartz shock temperature pyrometry standard to 4 TPa. *In prepara-*

tion for Phys. Rev. Lett.